# An Analytic and Experimental Comparison of Direct and External Modulation in Analog Fiber-Optic Links

CHARLES H. COX III, MEMBER, IEEE, GARY E. BETTS, MEMBER, IEEE, AND LEONARD M. JOHNSON, MEMBER, IEEE

*Abstract*—**Analytic lumped-element small-signal models of directly and externally modulated analog fiber-optic links have been derived. Incremental modulation efficiency is defined and used to compare the performance of these modulation techniques. In experiments to optimize link RF-to-RF gain and noise figure, the measurements obtained agreed with calculations to within ≈ 1 dB. The externally modulated link was operated with two different impedance matching circuits. With a low-pass match the bandwidth was 150 MHz, and the link transducer gain was 1 dB; with a band-pass match the bandwidth was 22 MHz, the link transducer gain was 11 dB, and the noise figure was 6 dB. The directly modulated link was operated with a low-pass match. In this case, the bandwidth was 1 GHz, the link transducer gain was −14 dB, and the noise figure was 33 dB. These experimental results were achieved with no amplification and represent a significant improvement in performance over previously reported analog fiber-optic links.**

## I. Introduction

FIBER-OPTIC links are being used increasingly to replace conventional guided-wave methods of conveying RF signals. A primary reason for this is that the optical fibers offer many advantages, such as low loss, high bandwidth, and low weight. Unfortunately, these advantages are masked by limitations of the RF-to-optical and optical-to-RF conversion processes. For example, although the fiber loss may be less than 1 dB/km, the RF-to-optical and optical-to-RF conversion typically results in a zero-length link transducer loss of 20 to 50 dB for directly modulated links and 30 to 60 dB for externally modulated links.

The basic link topologies using direct and external (or indirect) modulation are shown in Fig. 1. In direct modulation the RF signal modulates the intensity of the optical output of the laser directly. All directly modulated links use diode lasers, since this is the only type that at present offers sufficient bandwidth in a simple modulation interface. In an externally modulated link, the laser operates CW, with the intensity of its optical output modulated by the application of the RF signal to the modulator. Since modulation does not occur at the laser, in theory any laser of the appropriate wavelength can be used as a source. In fact, it will be shown that, for some links, lasers other than presently available diode lasers offer improved performance. The modulation function in externally modulated links can be implemented by various methods, such as a Mach–Zehnder (MZ) interferometer, a directional coupler, or a waveguide cutoff modulator.

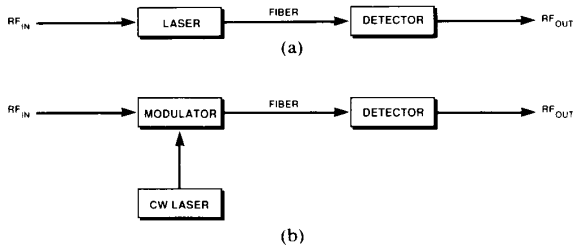


Fig. 1. Block diagrams of fiber-optic links using (a) direct modulation and (b) external modulation.

Previous comparisons of direct and external modulation have been primarily experimentally based [1], [2]. In this study, we provide a theoretical framework for link performance, which discriminates between differences that are inherent in the two types of links and those that are due to the choice of implementation. In our analysis, the link transducer power gain, $G$, is expressed as the product of three separately determinable components:

$$G = \frac{p_{\text{out}}}{p_{\text{in},a}} = \frac{p_o^2}{p_{\text{in},a}} t_{od}^2 \frac{p_{\text{out}}}{p_{od}^2} \tag{1}$$

where $p_{\text{out}}$ is the RF power delivered to the load at the link output, $p_{\text{in},a}$ is the available power from the RF source at the link input, $p_o$ is the fiber-coupled modulated optical power from the modulating device, $t_{od}$ is the link optical transfer efficiency ($t_{od} = p_{od}/p_o$), and $p_{od}$ is the modulated optical power in the photodetector fiber. The optical powers are squared in (1), because for the electro-optic devices under consideration the optical power is proportional to either RF voltage or current. The transfer efficiency, $t_{od}$, includes all factors affecting the transmission of light in the fiber from the modulating device to the detector. The expression of the link transfer function in (1) is useful because it permits flexibility in evaluating links comprising a variety of modulation and detection implementations. The first and third expressions in (1) describe

Manuscript received August 1, 1989; revised January 2, 1990. This work was supported by the Department of the Air Force.

The authors are with the Lincoln Laboratory, Massachusetts Institute of Technology, Lexington, MA 02173-9108.

IEEE Log Number 9034628.

0018-9480/90/0500-0501$01.00 ©1990 IEEE

the incremental modulation efficiencies. These efficiencies are useful both for evaluating the performance of the various electro-optic devices and for comparing the performance of several implementations of a given link function, such as source modulation.

In the following sections, we derive small-signal models for a directly modulated diode laser, a MZ external modulator, and a p-i-n photodiode. Link models based on these device models are then used to calculate link gain and noise figure. Finally, the results of experimental measurements on directly and externally modulated links are presented and compared with the calculated results. Our analysis excludes pre- or postamplification since the focus here is on the intrinsic capabilities of the links. However, the performance of a combination consisting of an amplifier and an optical link can be determined from our results, since the optical links are characterized in terms of the conventional RF parameters of transducer gain, noise figure, and bandwidth.

In our analysis, it will be necessary to express total instantaneous variables as the sum of an operating-point variable plus a small-signal variable. Thus, we have adopted a commonly used convention [3] of denoting operating-point variables by uppercase symbols and subscripts, small-signal instantaneous variables by lowercase symbols and subscripts, and total instantaneous variables by lowercase symbols and uppercase subscripts.

## II. Small-Signal Device Models

### A. Directly Modulated Diode Laser

A representative plot of the fiber-coupled optical power $p_O$ versus laser current $i_L$ for a directly modulated diode laser is shown in Fig. 2(a). In general, $p_O$ is related to $i_L$ by the slope efficiency $\eta_L$, given as [4] $\eta_L(i_L) = dp_O/di_L$. For efficient linear modulation, the bias current $I_L$ must be greater than the lasing threshold current $I_T$. The modulation current $i_l$ is superimposed on $I_L$, resulting in a total laser current $i_L = I_L + i_l$. If $i_l \ll I_L$, then $\eta_L(i_L) \cong \eta_L(I_L) \equiv \eta_{LB}$, where $\eta_{LB}$ is the slope efficiency independent of $i_l$. Under these conditions, the small-signal model for a diode laser is simply $p_o = \eta_{LB} i_l$, which states that about an operating point $I_L$, the laser can be modeled as a current-dependent optical power source. Consequently, the goal of the impedance matching circuit should be to maximize the modulating current through the laser.

Reasonably detailed lumped-element small-signal models of diode lasers have already been reported. At frequencies well below the relaxation resonance [4], the frequency response of the laser is dominated by two lumped elements: the resistance in series with the junction, $R_L$, and the bond wire inductance, $L_L$. Since $L_L$ is not a device parameter, it can be optimized independently of the laser design. The circuit model shown in Fig. 2(b) includes the laser, an ideal transformer, and the RF source represented by an ideal voltage source $v_{\text{in}}$ and a resistor $R_{\text{IN}}$. It can be shown that for $I_L > I_T$ the incremental voltage drop across the diode laser junction is negligible compared with the incremental voltage drop across $R_L$ [4]. With this approximation, a straightforward circuit analysis yields the following relation[1] between $p_o$ and $v_{\text{in}}$:

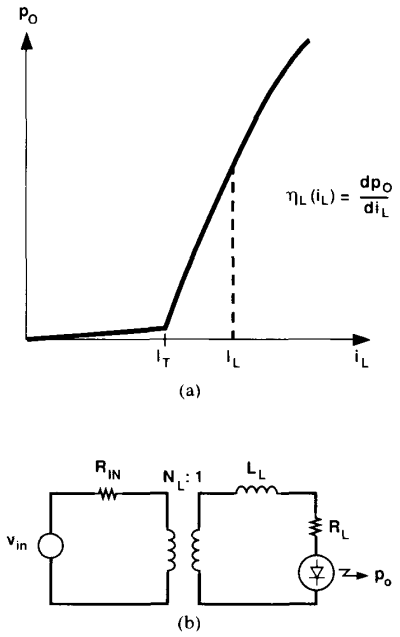


Fig. 2. (a) Optical power $p_O$ versus laser current $i_L$ for a diode laser and (b) small-signal lumped-element circuit model showing RF source, matching transformer, and diode laser.

$$p_o = \frac{\eta_{LB} N_L}{R_{T1}\left[\left(sN_L^2 L_L / R_{T1}\right) + 1\right]} v_{\text{in}} \tag{2}$$

where $N_L$ is the turns ratio of the laser transformer, $R_{T1} = N_L^2 R_L + R_{\text{IN}}$, and $s$ is the complex frequency.[2] The RF power available from the source $p_{\text{in},a}$ is

$$p_{\text{in},a} = \frac{v_{\text{in}}^2}{4R_{\text{IN}}}. \tag{3}$$

Dividing the square of (2) by (3) yields the incremental modulation efficiency for a diode laser:

$$\frac{p_o^2}{p_{\text{in},a}} = \frac{4R_{\text{IN}}\eta_{LB}^2 N_L^2}{R_{T1}^2\left[\left(sN_L^2 L_L / R_{T1}\right) + 1\right]^2}. \tag{4}$$

[1]Although (2) indicates a finite response at dc, a transformer-coupled circuit, of course, has no response at dc. Rather than limit the scope of the analysis, we chose to extend the implementations represented by the schematic symbol for the transformer. Response to dc can be implemented using the above analysis by replacing the transformer with a current-controlled current source (CCCS) having an output-to-input current ratio equal to the transformer turns ratio. Therefore, the transformer symbol will be used to represent implementation with both an actual transformer and a CCCS.

[2]The complex frequency $s$ can be represented by $\alpha + j\omega$, where $\alpha$ and $j\omega$ correspond to the real and imaginary parts, respectively. To evaluate the magnitude of the frequency response, one would set $\alpha = 0$. However, expressing equations in terms of the complex frequency makes it possible to evaluate the response of the device to more general inputs, e.g., a step input.

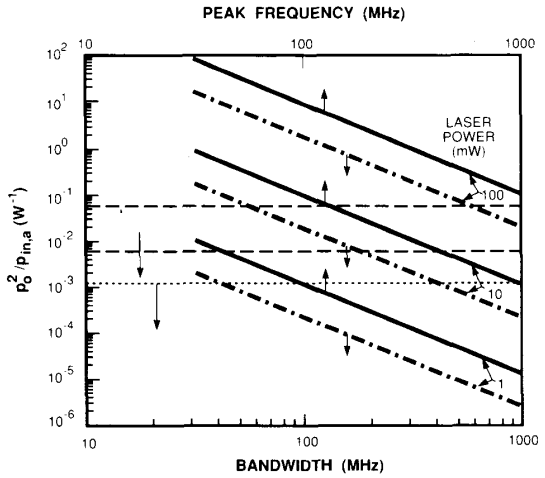


Fig. 3. Incremental modulation efficiency versus bandwidth for direct modulation (dashed line) and for external modulation with parallel matching (dotted and dashed line); incremental modulation efficiency versus peak frequency for external modulation with series matching (solid line).

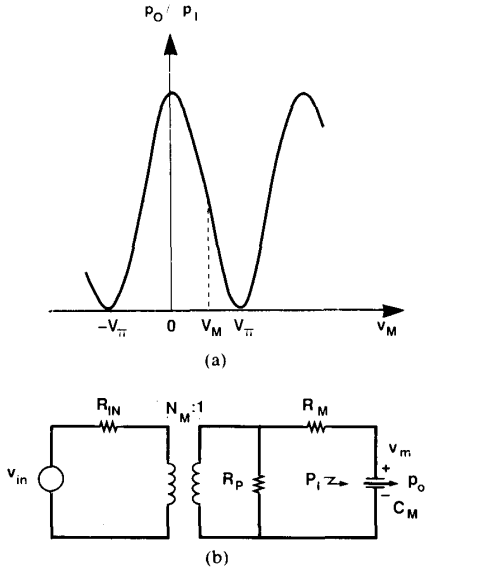


Fig. 4. (a) Optical transfer function $p_O/p_I$ versus voltage $v_M$ for a MZ external modulator and (b) small-signal lumped-element circuit model showing RF source, matching transformer, and MZ modulator.

When $R_L$ is matched to $R_{IN}$ via $N_L(N_L^2 R_L = R_{IN})$, equation (4) reduces to

$$\left(\frac{p_o^2}{p_{in,a}}\right)_M = \frac{\eta_{LB}^2}{R_L\left[(sL_L/2R_L)+1\right]^2} \tag{5}$$

with the subscript $M$ denoting this matching condition. It is evident from (5) that to maximize the magnitude of this transfer function and thereby reduce link RF-to-RF insertion loss, one wants to maximize $\eta_{LB}$ and minimize $R_L$, to the extent possible, while still matching $R_L$ to $R_{IN}$. To maximize the bandwidth of (5) requires minimizing $L_L$, a package parameter, and maximizing $R_L$. Thus, $R_L$ is the only parameter for which a trade-off exists between gain and bandwidth. Some fundamental limits of the impedance matching versus bandwidth trade-offs are explored in [5].

The values for modulation efficiency can be obtained by substituting in (5) representative values of present diode lasers. Fiber-coupled laser slope efficiencies are typically 0.025 W/A for uncoated lasers and 0.040 W/A for lasers with asymmetrical coatings. (These slope efficiencies are well below the theoretical limit for a laser without a fiber because laser-to-fiber coupling efficiency is typically less than 10%.) The series resistance ranges from 3 to 12 Ω. If it is assumed that $L_L$ is small enough so as not to limit the bandwidth, then the incremental modulation efficiency has no bandwidth dependence. Modulation efficiency as obtained from (5) for the ranges of values given above is represented by the shaded area in Fig. 3.

All commercially available impedance-matched lasers use a resistor $R_{L1}$ in series with $R_L$, with $R_{L1}$ chosen such that $R_{L1} + R_L = R_{IN}$. The resistive match is a simple approach, offering the widest bandwidth for a given $L_L$, although at reduced modulation efficiency. Modulation efficiency for the resistive match case obtained from (5), by letting $N_L = 1$ and $R_L = R_{IN}$, is represented by a dotted line in Fig. 3.

### *B. Balanced Mach–Zehnder (MZ) External Modulator*

The optical transfer function $p_O/p_I$ versus voltage $v_M$ for a MZ interferometric external modulator is shown in Fig. 4(a). In general, the fiber-coupled optical output $p_O$ from this modulator is related to the optical power in the input fiber, $p_I$, and the voltage applied to modulator electrodes, $v_M$, as follows [6]:

$$p_O = \frac{t_{ff} p_I}{2}\left(1 + \cos\frac{\pi v_M}{V_\pi}\right). \tag{6}$$

Here, $t_{ff}$ is the optical transmission from the input fiber to the output fiber when the interferometer is biased for maximum transmission, and $V_\pi$, which depends on specifics of the modulator design, is the voltage required to produce a differential phase shift $\pi$ between the interferometric modulator arms. For linear modulation, $v_M = V_M + v_m$, where $V_M$ is the bias voltage and $v_m$ is the desired modulation voltage. In principle, since the transfer function for these devices is periodic, any one of a number of values for $V_M$ could be used to achieve maximal small-signal response. Typically, the lowest positive value $V_\pi/2$ is used. For $V_M = V_\pi/2$ and $v_m \ll V_M$, the incremental transfer function for a MZ external modulator is

$$p_o = \frac{t_{ff} P_I}{2}\left(-\frac{\pi v_m}{V_\pi}\right). \tag{7}$$

Thus, to maximize the modulated optical power, the impedance matching circuit should maximize the transfer from $P_{in,a}$ to $v_m$. As was the case with the diode laser, maximizing the current through the modulator will maxi-

mize $v_m$. However, here $v_m$ is the voltage across a capacitor, so the frequency dependence will be different.

Fig. 4(b) is a lumped-element small-signal circuit model showing an RF source, ideal transformer, and MZ modulator [7]. The elements $R_M$ and $C_M$ represent the resistance and capacitance, respectively, of the modulator electrodes, and $R_P$ represents the resistive termination commonly used with these modulators. A straightforward circuit analysis yields the following relation between $p_o$ and $v_{\text{in}}$:

$$p_o = \frac{t_{ff} P_I \pi}{2V_\pi} \frac{N_M R_P}{R_{T2}} \frac{1}{sC_M R_{T3} + 1} v_{\text{in}} \tag{8}$$

where $N_M$ is the turns ratio of the modulator transformer, $R_{T2} = N_M^2 R_P + R_{\text{IN}}$, and $R_{T3} = [R_{\text{IN}}(R_P + R_M) + N_M^2 R_P R_M]/R_{T2}$. In general, RF matching would require that $R_{\text{IN}} = N_M^2 \,\text{Re}\{R_P \| [R_M + (sC_M)^{-1}]\}$, with Re denoting the real part of the bracketed expression. The matching options can be understood by considering two limiting cases of a parallel match where $N_M^2 R_P = R_{\text{IN}}$, and a series match where $N_M^2 R_M = R_{\text{IN}}$.

*1) Parallel Match:* A parallel match requires that $|R_M + (sC_M)^{-1}| \gg R_P$, which can be refined to $|sC_M|^{-1} \gg R_P$, since in general $R_M < R_P$. If this condition is used to simplify (8) and the result is squared and divided by (3), the incremental modulation efficiency is

$$\left(\frac{p_o^2}{p_{\text{in},a}}\right)_{M,P} \cong \left(\frac{t_{ff} P_I \pi}{2V_\pi}\right)^2 \frac{R_{\text{IN}}}{N_M^2} = \left(\frac{t_{ff} P_I \pi}{2V_\pi}\right)^2 R_P \tag{9}$$

with the subscripts $M, P$ denoting this parallel match. This case has a low-pass frequency response, which has traditionally been used with $N_M = 1$ and $R_P = R_{\text{IN}}$.

It is clear from (8) that the bandwidth of the modulation efficiency is proportional to $(R_P C_M)^{-1}$. It appears from (9) that the magnitude of the modulation efficiency depends only on $R_P$. However, $V_\pi$ is inversely proportional to the electrode length $L$, and $C_M$ is proportional to $L$ [8]. Substituting these proportionalities in (9), we see that the magnitude of the modulation efficiency is proportional to $R_P C_M^2$. Thus, both the magnitude and the bandwidth of the modulation efficiency are dependent on both $R_P$ and $C_M$. Consequently, for the parallel-matched MZ modulator a fundamental trade-off exists between modulation efficiency and bandwidth. Also, note that although the frequency response for a given bandwidth has a low-pass form, the envelope of the frequency responses at various bandwidths has an $s^{-2}$ dependence. This relation is evident in the plot of (9), shown in Fig. 3 for three values of laser power $P_I$, where $R_P = 50\ \Omega$, $C_M V_\pi = 24$ pC, and $t_{ff} = 1$. It is evident from Fig. 3 that for high optical power and low-to-moderate frequencies a MZ modulator with a parallel match will have a substantially higher modulation efficiency than a diode laser.

*2) Series Match:* The series match case, in which $R_P$ is omitted, requires that $|sC_M|^{-1} \ll R_M$. A straightforward way to achieve this is to operate the series-matched modulator at frequencies such that $\omega > (C_M R_M)^{-1}$. Using the above conditions to simplify (8) and then squaring the result and dividing by (3), we obtain the incremental modulation efficiency:

$$\left(\frac{p_o^2}{p_{\text{in},a}}\right)_{M,S} \cong \left(\frac{t_{ff} P_I \pi}{2V_\pi}\right)^2 \frac{N_M^2}{s^2 C_M^2 R_{IN}} = \left(\frac{t_{ff} P_I \pi}{2V_\pi}\right)^2 \frac{1}{s^2 C_M^2 R_M} \tag{10}$$

with the subscripts $M, S$ denoting this series match. Although (10) was derived for a specific circuit, it represents the optimum modulation efficiency for any passive matching circuit [8].

By combining the constraint on the valid range of operation, $\omega > (C_M R_M)^{-1}$, with the fact that (10) decreases as $\omega^2$, we see that the series-matched modulator has a band-pass frequency response. Since the series-matched frequency response is inherently band-pass, an alternative technique for achieving $|sC_M|^{-1} \ll R_M$ is to form a series resonant loop by adding an inductor in series with the $C_M - R_M$ loop. An advantage of this technique is that it permits series-matched operation at frequencies less than $(C_M R_M)^{-1}$.

The series-matched modulation efficiency as expressed by (10) is plotted in Fig. 3 for the same values as the parallel match case and with $R_M = 5\ \Omega$. Because of the band-pass frequency dependence, the modulation efficiency is plotted versus peak frequency rather than bandwidth. The trade-off between modulation efficiency and bandwidth becomes explicit if we recall that $C_M$ is proportional to $V_\pi^{-1}$. The magnitude of (10) depends on the $C_M V_\pi$ product, so maximizing the magnitude of (10) depends only on $R_M$ [8]. Bandwidth, of course, is still a function of $C_M R_M$ and, in the case with a series resonant inductor, a function of series inductance as well. Therefore, in the series match case one could choose $R_M$ to achieve the specified efficiency and then choose $C_M$ to obtain the required bandwidth without the choice of $C_M$ affecting the modulation efficiency.

### C. p-i-n Photodiode

Under reverse bias, the current that flows through a p-i-n photodiode, $i_D$, is related to the optical power incident on the photodetector, $p_{OD}$, via the slope efficiency [9]:

$$\eta_D = \frac{di_D}{dp_{OD}}. \tag{11}$$

As this relation is linear up to at least seven orders of magnitude, $\eta_D$ is independent of $p_{OD}$ in this range. Consequently, (11) holds true for incremental signals. Thus, the small-signal model of a reverse-biased photodiode is an optical-power-controlled current source. A first-order approximation of the frequency response requires the inclusion of two lumped elements, the diode junction shunt capacitance $C_D$ and the series resistance $R_D$. In the circuit shown in Fig. 5, these elements are connected to an ideal transformer, the output of which is terminated by an RF load $R_{\text{OUT}}$. A straightforward analysis of this circuit yields

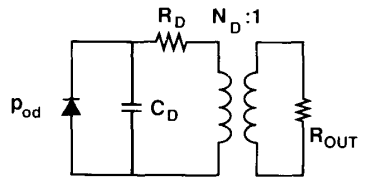


Fig. 5. Small-signal lumped-element circuit model showing p-i-n photodiode, matching transformer, and RF load.

the incremental modulation efficiency,

$$\frac{p_{\text{out}}}{p_{od}^2} = \frac{\eta_D^2 R_{\text{OUT}} N_D^2}{\left[sC_D\left(R_D + N_D^2 R_{\text{OUT}}\right)+1\right]^2} \tag{12}$$

where $N_D$ is the turns ratio of the photodiode transformer. As with the diode laser and MZ modulator, a clear trade-off exists between maximizing modulation efficiency by maximizing $N_D$ and simultaneously reducing bandwidth as a result of the increases in $N_D$. For $\omega < [C_D(R_D + N_D^2 R_{\text{OUT}})]^{-1}$, equation (12) reduces to

$$\frac{p_{\text{out}}}{p_{od}^2} = \eta_D^2 R_{\text{OUT}} N_D^2. \tag{13}$$

For the link calculations presented below, we will need to evaluate (13) using typical values for present photodiodes. At a wavelength of 1.3 $\mu$m, we can assume $\eta_D = 0.8$. We also assume that the detector has a 75-$\mu$m-diameter active area, which typically results in $C_D = 0.5$ pF. If we take $N_D = 1$, $R_D = 0$, and $R_{\text{OUT}} = 50\ \Omega$, then for frequencies less than 6 GHz $p_{\text{out}}/p_{od}^2 = 32\ \text{mW}^{-1}$.

## III. Small-Signal Link Models

The device models presented in the previous section can be combined to form small-signal link models, which in turn can be used to calculate a number of link parameters. The two parameters discussed here are link gain and noise figure. Plots of link gain versus laser power and of noise figure versus laser power are shown in parts (a) and (b) of Fig. 6, respectively.

Models for link gain in terms of various device parameters are obtained by substituting in (1) the expressions derived above for small-signal modulation efficiency of the diode laser or MZ modulator and photodetector. In the calculations that follow, we assume that the modulating device is matched to the RF source resistance and that for devices with a low-pass frequency response the link is operating at less than the 3 dB frequency. For a directly modulated link, substitution of (5) and (13) into (1) yields

$$G = \frac{1}{R_L}\eta_{LB}^2 t_{od}^2 \eta_D^2 R_{\text{OUT}} N_D^2. \tag{14}$$

For an externally modulated link, $G$ depends on the matching option. With a parallel match, substituting (9) and (13) into (1) gives

$$G = R_P\left(\frac{t_{ff} P_I \pi}{2V_\pi}\right)^2 t_{od}^2 \eta_D^2 R_{\text{OUT}} N_D^2. \tag{15}$$

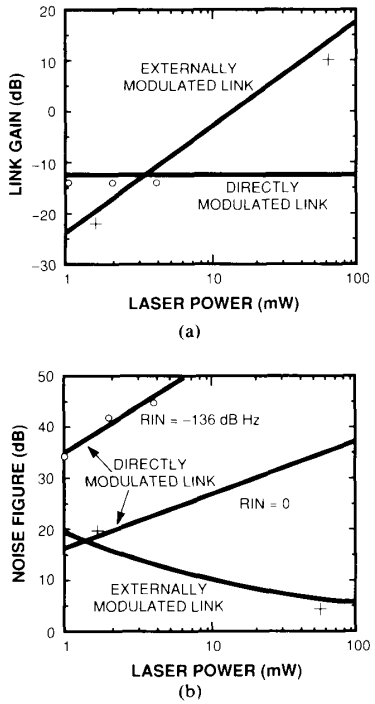


Fig. 6. (a) RF gain versus laser power and (b) noise figure versus laser power. Plotted are calculated values for directly and externally modulated links (solid lines), experimental data for the directly modulated link (circles), and experimental data for the externally modulated link (crosses).

With a series match, substitution of (10) and (13) into (1) yields

$$G = \frac{1}{s^2 C_M^2 R_M}\left(\frac{t_{ff} P_I \pi}{2V_\pi}\right)^2 t_{od}^2 \eta_D^2 R_{\text{OUT}} N_D^2. \tag{16}$$

There are two important distinctions between equation (14) and equations (15) and (16). In (14), $G$ is independent of the optical bias power, and $\eta_{LB}^2$ has an upper bound determined by conservation of energy. By contrast, in (15) and (16) $G$ increases as the square of the optical bias power, and the term $(t_{ff} P_I \pi / 2V_\pi)^2$, which is analogous to $\eta_{LB}^2$ in (14), in principle has no upper bound although it may be limited by such factors as the maximum optical power density of the waveguide. Results of calculations of (14) and (16) using the device parameters listed in Table I are plotted in Fig. 6(a). The gain of the two links is equal at a laser power of $\approx 3$ mW. It is interesting to note that for laser powers above $\approx 13$ mW, the insertion loss for the externally modulated link is completely overcome, resulting in a net gain. With sufficient laser power, this gain can be as high as 10 to 20 dB.

Another important measure of link performance is the noise figure, $NF$, expressed as

$$NF = 10 \log \frac{N_O}{N_I G} \tag{17}$$

TABLE I
PARAMETERS USED IN CALCULATIONS FOR SMALL-SIGNAL LINKS

| Element | Symbol | Value | Unit |
|---|---|---|---|
| Direct modulation | | | |
| Slope efficiency | $\eta_{LB}$ | 0.14 | W/A |
| Laser series resistance | $R_L$ | 12.5 | Ω |
| Link optical transfer efficiency | $t_{od}$ | 1 | |
| External modulation | | | |
| Modulator capacitance | $C_M$ | 45 | pF |
| Modulator resistance | $R_M$ | 16 | Ω |
| Resistive termination | $R_P$ | 50 | Ω |
| Modulator switching voltage | $V_\pi$ | 0.7 | V |
| Optical power in input fiber to modulator | $P_I$ | 55 | mW |
| Frequency | | 52 | MHz |
| Modulator maximum optical transmission | $t_{ff}$ | 0.35 | |
| Link optical transfer efficiency | $t_{od}$ | 1 | |

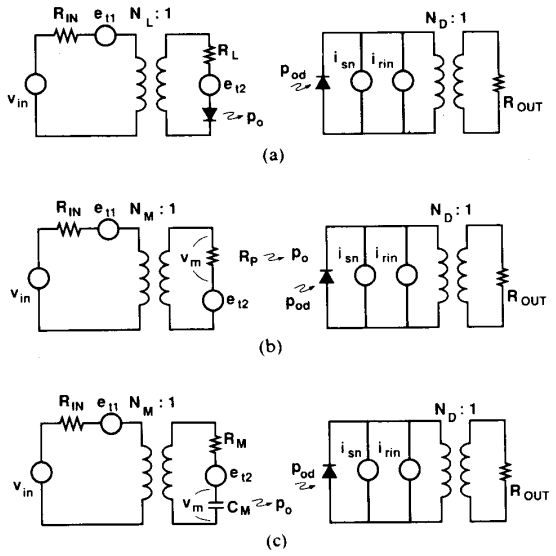


Fig. 7. Circuit models showing dominant noise sources in (a) directly modulated link, (b) externally modulated link with parallel match, and (c) externally modulated link with series match.

where $N_O$ is the total available noise power at the link output and $N_I$ is the available thermal noise power at the link input. The dominant noise sources for the link models are shown in Fig. 7. These include the thermal noise of the resistive component of the source, $e_{t1}$, and modulator, $e_{t2}$; the shot noise at the photodetector, $i_{sn}$; and the relative intensity noise of the laser, $i_{rin}$. For the range of optical bias powers considered here, the thermal noise of the output load $R_{\mathrm{OUT}}$ is negligible compared with the shot noise and has been omitted. For the circuits shown in Fig. 7,

$$NF = 10\log\left[1 + \frac{N^2 e_{t2}^2}{e_{t1}^2} + \frac{4R_{\mathrm{IN}}R_{\mathrm{OUT}}N_D^2}{e_{t1}^2 G}\left(i_{sn}^2 + i_{rin}^2\right)\right] \quad (18)$$

where $N$ is the turns ratio for matching the RF source into the laser or modulator. An important special case occurs when the laser or modulator resistance $R$ is matched to the RF source and the RF source is matched to the load, given as $N^2R = R_{\mathrm{IN}} = R_{\mathrm{OUT}}$. Applying this condition to (18) results in

$$NF = 10\log\left[2 + \frac{N_D^2 R_{\mathrm{IN}}}{kTG}\left(i_{sn}^2 + i_{rin}^2\right)\right] \quad (19)$$

where $k$ is Boltzmann's constant and $T$ is the absolute temperature. The constant 2, which corresponds to a noise figure of 3 dB, represents the fundamental limit for a passively matched input. Clearly, increases in the link gain are necessary for $NF$ to approach the 3 dB limit.

The dependence of noise figure on link type and device parameters can be seen in Fig. 6(b), which plots link noise calculated from (19) versus laser optical power. The required values for link gain were calculated from (14) and (16) for directly and externally modulated links, respectively. It is assumed that the laser RIN is negligible compared with the shot noise, which is a good approximation for solid-state lasers at RF frequencies, and an optimistic but not unattainable goal for diode lasers. For a directly modulated link, the noise figure increases with increasing laser power, because the link gain is independent of laser power while the photodetector shot noise increases linearly with laser power. Conversely, for an externally modulated link the noise figure decreases with increasing laser power because, despite the linearly increasing shot noise, the link gain increases as the square of the laser power. Consequently, the effects of shot noise at the photodetector on the link noise figure in an externally modulated link can in principle be reduced to arbitrarily low levels although, because of the resistive component of the modulator input, the minimum link noise figure is limited to 3 dB.

The optical power at which gain for directly and externally modulated links is the same, shown in Fig. 6(a), depends directly on the device parameters used in the calculations. For example, with improved laser slope efficiency the optical power required for the links to have the same gain will be higher. However, the general trends represented in Fig. 6 are, at least to the first order, independent of the values of the device parameters. Thus, over a wide range of implementations, increasing the optical power will result in increased gain and decreased noise figure for an externally modulated link and a constant gain and increased noise figure for a directly modulated link.

## IV. EXPERIMENTAL RESULTS

### A. Directly Modulated Fiber-Optic Link

Our directly modulated link had an InGaAsP/InP buried double-heterostructure diode laser [10] operating at 1.3 μm. The RF input was passed through a wide-band 4:1 step-down transformer to a dc blocking capacitor to the laser. The optical output from the laser was coupled directly into a 50/125 μm graded-index multimode fiber with one end rounded to form a lens, giving a laser-to-fiber coupling efficiency of 0.7. The RF output from the photodiode was passed through a bias network and terminated in a 50 Ω load. No resistive back termination was used across the photodiode; nor was there a matching trans-

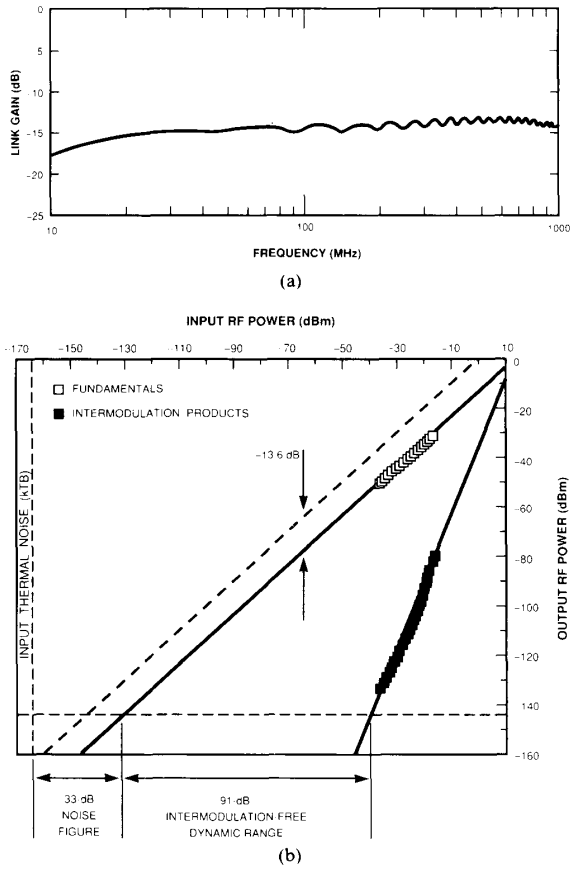


Fig. 8. Experimental results using directly modulated fiber-optic link. (a) Link transducer gain versus frequency. (b) Fundamental and two-tone intermodulation distortion link outputs versus fundamental link input power.

former between the photodiode and the output load resistor.

The link insertion gain versus frequency plotted in Fig. 8(a) was measured using a network analyzer with the laser bias power set at 1 mW. The roll-off below 20 MHz was due to the dc blocking capacitor. The measured insertion gain, plotted as circles in Fig. 6(a), was approximately the same with the laser biased at 1, 2, and 4 mW and was $\approx 1$ dB lower than the calculated values. This demonstrated that the link model has sufficient detail to predict the dominant link parameters, since the device parameters of the links used in the experiments corresponded to those used in the calculations.

Measurements of the two-tone intermodulation (IM) power with the laser bias power set at 1 mW are shown in Fig. 8(b). The input and output noise levels are indicated by the lightly dashed lines, and the unity gain by the bold dashed line. The noise bandwidth was intentionally narrow (10 Hz) so that the IM powers could be measured over a wide range of RF input powers. Plots of the measured noise figure values do not agree well with the calculated link noise figures shown in Fig. 6(b). This is because the calculated values were obtained assuming a negligible diode laser RIN, whereas the measured RIN was $-136$ dB/Hz, which is a reasonable value for this type of laser and these operating conditions. If we include this value of RIN in the noise figure calculation, there is good agreement between measured and calculated values.

### *B. Externally Modulated Fiber-Optic Link*

Our MZ external modulator was fabricated in $LiNbO_3$ with Ti-indiffused waveguides. The modulator electrodes were 55 mm long, resulting in a $V_\pi$ of 0.7 V [11]. The RF input to the link was either parallel matched to the modulator electrodes with a 50 $\Omega$ resistor or passed through a double-tuned circuit to the modulator electrodes in a series match. The optical source was a diode-laser-pumped Nd:YAG solid-state laser designed to operate at 1.32 $\mu$m (a secondary line of Nd:YAG). The laser output was passed through an optical isolator and then focused into a single-mode polarization-maintaining fiber, which was end-fire coupled directly to the input waveguide of the modulator. The fiber-to-fiber optical insertion loss was 4.5 dB with the interferometer biased for maximum transmission ($t_{ff} = 0.35$). A second fiber, also end-fire coupled, was used to transfer the output of the modulator into a photodiode having virtually identical specifications to the one used in the directly modulated link experiments.

A measurement was made of the link frequency response with 55 mW of laser power [12] in the input fiber to the modulator. The results for both parallel and series match cases are shown in Fig. 9(a). Note that the link gain is represented on an absolute rather than a relative or normalized scale. With a parallel match on the modulator input, the link had a net gain of slightly less than 1 dB, and the bandwidth was $\approx 150$ MHz. With a series match, the bandwidth was $\approx 22$ MHz, and the peak gain increased to 11 dB. This 11 dB gain and a comparable measurement obtained with 1.5 mW optical power are plotted in Fig. 6(a). As can be seen, the measured values agree with the calculated values to within $\approx 1$ dB.

The different bandwidths of the experimental links do not preclude comparison of gain in directly and externally modulated links. Operation of the directly modulated link at a narrower bandwidth would not be expected to produce any significant improvement in link performance because the wide-band matching has already maximized the current through the laser. On the other hand, although the operation of the externally modulated link at a wider bandwidth or higher center frequency decreases the peak gain, the gain is easily estimated since it increases in proportion to the square of the frequency decrease because of the capacitive impedance of the MZ modulator.

Results of two-tone IM measurements on the externally modulated link [12] operating with 55 mW optical power are plotted in Fig. 9(b). The IM-free dynamic range in a 10 Hz noise bandwidth was 104 dB, which is 13 dB larger than for the directly modulated link and occurs at $\approx 10$ dB lower RF input power. However, this is not a fundamental distinction since the input power for maximum IM-free

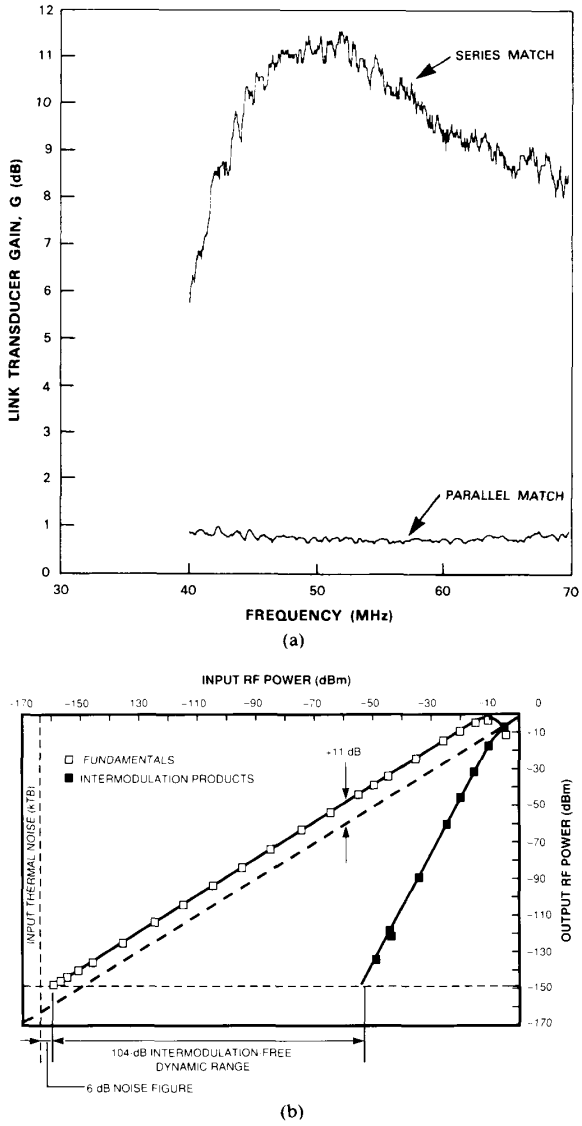


Fig. 9. Experimental results using externally modulated fiber-optic link. (a) Link transducer gain versus frequency with parallel and series matches. (b) Fundamental and two-tone intermodulation distortion link outputs versus fundamental link input power with a series match.

dynamic range is a function of modulator design. The noise figure was 6 dB, which is a substantial improvement over the directly modulated link. Decreasing the optical power to 1.5 mW increased the noise figure to 21 dB. Both data points are plotted in Fig. 6(b) and agree well with calculated values, which is a confirmation that the solid-state laser RIN is negligible at these frequencies.

## V. Conclusions

We have derived and compared incremental modulation efficiency for directly and externally modulated analog fiber-optic links using various device parameters. It was found that the efficiency of a MZ external modulator operated at moderate bandwidths and with high optical power may be several orders of magnitude greater than that of a directly modulated diode laser. We also examined the effect of impedance matching of the electro-optic devices. Despite different load impedances, in both modulation techniques the insertion loss was minimized by maximizing the current through the devices. Further, it was demonstrated that both narrow-band and broad-band nondissipative impedance matching of any of the electro-optic devices can be effective in reducing the link insertion loss, despite differences in the type of frequency response and bandwidth for the two modulation methods.

For externally modulated links, the fact that link insertion gain is proportional to the square of the optical bias power has at least two important consequences. First, it permits substantial reduction or even elimination of the RF-to-RF insertion loss. For modulators with predominately capacitive input impedance, such as the MZ, the maximum modulation efficiency is inversely proportional to the square of the frequency. Therefore, in terms of insertion loss, externally modulated links have the greatest advantage over directly modulated links at low-to-moderate frequencies. Second, it allows suppression of the contribution of photodetector shot noise. Thus, with sufficiently high optical bias power the noise figure of the externally modulated link can be substantially lower than that of the directly modulated link. The link type selected for a particular application will depend on such parameters as IM-free dynamic range, which may in turn affect the choice of specific device parameters. However, for a wide range of applications, the functional distinctions between the two types of links will be independent of the specific implementation.

## Acknowledgment

The authors thank R. C. Williamson and D. L. Spears for helpful discussions, Z. L. Liau and J. N. Walpole for use of the semiconductor lasers, G. A. Rezendes, R. D. Glenn, and K. G. Ray for assistance in the setup of the links used in the experiments, H. V. Roussell and A. C. Yee for data collection and reduction, K. J. Challberg for editorial assistance, and N. A. Blue and L. G. Korn for manuscript preparation.

## References

[1] C. M. Gee, I. L. Newberg, G. D. Thurmond, and H. W. Yen, "X-band rf fiber optic links," *Proc. SPIE*, vol. 716, pp. 64–68, 1986.

[2] W. E. Stephens and T. R. Joseph, "System characteristics of direct modulated and externally modulated RF fiber-optic links," *J. Lightwave Technol.*, vol. LT-5, pp. 380–387, 1987.

[3] P. E. Gray and C. L. Searle, *Electronic Principles: Physics, Models, and Circuits*. New York: Wiley, 1969, front matter, p. xx.

[4] G. P. Agrawal and N. K. Dutta, *Long-Wavelength Semiconductor Lasers*. New York: Van Nostrand Reinhold, 1986, pp. 23–69, 184–186, and 256–263.

[5] R. V. Schmidt, "Integrated optics switches and modulators," in *Integrated Optics: Physics and Applications*, S. Martellucci and A. N. Chester, Eds. New York: Plenum, 1987.

[6] R. A. Becker, "Broad-band guided-wave electrooptic modulators," *IEEE J. Quantum Electron.*, vol. QE-20, pp. 723–727, 1984.

[7] L. M. Johnson, "Relative performance of impedance-matched lumped-element and traveling-wave integrated-optical phase modulators," *IEEE Photon. Technol. Lett.*, vol. 1, pp. 102–104, 1989.
[8] J. M. Senior, *Optical Fiber Communications: Principles and Practice*. Englewood Cliffs, NJ: Prentice-Hall, 1985, ch. 8.
[9] Z. L. Liau and J. N. Walpole, "A novel technique for GaInAsP/InP buried heterostructure laser fabrication," *Appl. Phys. Lett.*, vol. 40, pp. 568–570, 1982.
[10] G. E. Betts, L. M. Johnson, and C. H. Cox, "High sensitivity lumped-element bandpass modulators in $LiNbO_3$," *J. Lightwave Technol.*, to be published.
[11] G. E. Betts, L. M. Johnson, C. H. Cox III, and S. D. Lowney, "High performance optical analog link using an external modulator," in *CLEO Tech. Dig.*, vol. 11, 1989, paper TUJ19.
[12] M. de La Chapelle, J. J. Gulick, and H-P. Hsu, "Analysis of low loss impedance matched fiber-optic transceivers for microwave signal transmission," *Proc. SPIE*, vol. 716, pp. 120–125, 1986.

**Charles H. Cox III** (S'66–M'70) received the B.S.E.E. and M.S.E.E. degrees in 1970 and 1972, respectively, from the University of Pennsylvania, Philadelphia. He received the Sc.D. degree from the Massachusetts Institute of Technology, Cambridge, MA, in 1979.

Since 1979 he has been a Member of the Technical Staff of M.I.T. Lincoln Laboratory. From 1979 to 1981 he was in the Photovoltaic Systems Group, where his research interests included PV cells, power circuits, and array interface modeling. Since 1981 he has been in the Applied Physics Group, where his research has focused on the modeling and application of high-speed semiconductor diode lasers, optoelectronic switches, and external modulators, as well as on new applications of fiber and integrated-optic devices.

Dr. Cox is a member of the Optical Society of America and Sigma Xi.

**Gary E. Betts** (S'84–M'84) was born in Seattle, WA, on May 14, 1954. He received the B.S. degree in physics from Haverford College, Haverford, PA, in 1976 and the M.S. degree in physics, and the Ph.D. degree in applied physics from the University of California at San Diego in 1980 and 1985, respectively. His thesis work dealt with electro-optic modulators in lithium niobate.

From 1976 to 1978 he worked in integrated optics, primarily in the design of geodesic lenses, at the Westinghouse Electric Corporation, Baltimore, MD. since 1985 he has been a Staff Member at the M.I.T. Lincoln Laboratory, Lexington, MA, working on lithium niobate integrated-optical devices, primarily microwave-frequency modulators and modulators for analog optical links.

Dr. Betts is a member of the Optical Society of America and the IEEE Lasers and Electro-Optics Society.

**Leonard M. Johnson** (S'75–M'81) was born in Arlington, MA, on June 4, 1954. He received the S.B., S.M., and Ph.D. degrees, all in electrical engineering, from the Massachusetts Institute of Technology, Cambridge, MA, in 1976, 1978, and 1981, respectively.

Since 1981 he has been a Staff Member in the Applied Physics Group of the Solid State Division of M.I.T. Lincoln Laboratory. He has worked primarily on the development of $LiNbO_3$ integrated optical devices including high-speed modulators and optical frequency shifters for signal-processing and fiber-sensor applications. He is currently involved with the development of novel waveguide modulators for wide-dynamic-range analog optical links.